Multi-target spectrally resolved fluorescence lifetime imaging microscopy

Thomas Niehörster[1], Anna Löschberger[1], Ingo Gregor[2], Benedikt Krämer[3], Hans-Jürgen Rahn[3], Matthias Patting[3], Felix Koberling[3], Jörg Enderlein[2] & Markus Sauer[1]

We introduce a pattern-matching technique for efficient identification of fluorophore ratios in complex multidimensional fluorescence signals using reference fluorescence decay and spectral signature patterns of individual fluorescent probes. Alternating pulsed laser excitation at three different wavelengths and time-resolved detection on 32 spectrally separated detection channels ensures efficient excitation of fluorophores and a maximum gain of fluorescence information. Using spectrally resolved fluorescence lifetime imaging microscopy (sFLIM), we were able to visualize up to nine different target molecules simultaneously in mouse C2C12 cells. By exploiting the sensitivity of fluorescence emission spectra and the lifetime of organic fluorophores on environmental factors, we carried out fluorescence imaging of three different target molecules in human U2OS cells with the same fluorophore. Our results demonstrate that sFLIM can be used for super-resolution multi-target imaging by stimulated emission depletion (STED).

Fluorescence microscopy is the method of choice for the visualization of biomolecules in fixed and living cells because it allows the selective and specific detection of molecules with high signal-to-background ratios[1]. Confocal scanning microscopy[2,3] and two-photon microscopy[4] enable optical sectioning and three-dimensional imaging deep inside living samples, providing insights into structure-function relationships. These revolutionary improvements came with the development of genetically encoded fluorophores, such as GFP and its derivatives[5,6], as well as chemical tags for live-cell labeling with organic fluorophores[7,8]. With specific and efficient fluorescent probes spanning a large spectral range[9], researchers can image almost any kind of cellular component, sometimes with single-molecule sensitivity[10,11].

Being able to study multiple interactions at the same time with a single measurement is of utmost importance in biology and medicine. Therefore, multiplexing and multidimensional microscopy of different target molecules in parallel is a powerful approach. If multiple fluorophores are to be used simultaneously, their fluorescence characteristics have to differ clearly in order for them to be identified unequivocally. Besides fluorescence polarization, which has been used mainly in homogeneous binding assays[12], multi-target fluorescence imaging of immunofluorescently stained cells is commonly accomplished by means of spectrally resolved detection and multicolor analysis[13–15] or via time-resolved detection by fluorescence lifetime imaging microscopy[16–20] (FLIM). Successful use of these two techniques in combination (i.e., sFLIM) has also been demonstrated at the ensemble and single-molecule levels[21–25].

At present, multicolor analysis of different fluorophores is mainly achieved via filter-based isolation of fluorescence signals. Therefore, researchers typically select fluorophores that exhibit minimal spectral overlap to ease data analysis. However, Fourier spectroscopy–based hyperspectral imaging and singular value decomposition have been used[15] for resolving overlapping emission spectra of immunofluorescently stained tissue samples, and efficient pattern-matching algorithms have been introduced[26–28] for the identification of different fluorophores on the basis of their characteristic fluorescence decay. These algorithms are applicable to arbitrary fluorescence-decay behavior and do not assume any knowledge of the underlying nature. In addition, identification of three different fluorescent probes has been achieved with spectrally resolved frequency-domain FLIM using a phasor approach[29,30]. Gerritsen and coworkers presented an analysis scheme based on the computation of spectral phasors[31] and use of a time-domain sFLIM instrument[25] to demonstrate unmixing of three dyes.

Here we present a novel sFLIM technique for multi-target fluorescence imaging based on confocal sample scanning with pulsed interleaved excitation at 485 nm, 532 nm and 640 nm and time-correlated single-photon counting (TCSPC) on 32 spectrally separated detection channels. On the basis of previous work[20], we developed a pattern-matching algorithm for efficient determination of the contribution of each fluorophore per pixel in complex multidimensional fluorescence signals. This algorithm is improved by the combined use of spectral and temporal information in the pattern-based analysis. The algorithm uses reference patterns of fluorescence decay and spectral signatures obtained from cell samples labeled with different fluorescent probes. The technique enables unequivocal identification of the signals

[1]Department of Biotechnology & Biophysics, Julius Maximilian University of Würzburg, Würzburg, Germany. [2]Drittes Physikalisches Institut, Georg-August-Universität, Göttingen, Germany. [3]PicoQuant GmbH, Berlin, Germany. Correspondence should be addressed to M.S. (m.sauer@uni-wuerzburg.de).

RECEIVED 17 AUGUST 2015; ACCEPTED 16 DECEMBER 2015; PUBLISHED ONLINE 25 JANUARY 2016; DOI:10.1038/NMETH.3740

of five green, five yellow or five red fluorophores with very similar fluorescence-emission characteristics. Furthermore, with this technique even slight changes in the fluorescence-emission characteristics of a fluorophore when attached to different biomolecules (e.g., antibodies) due to slight variations in the local environment can be used for specific fluorescence imaging of different cellular components. Finally, we show that sFLIM enables super-resolution fluorescence imaging of two spectrally similar fluorophores by STED microscopy[32].

RESULTS

sFLIM with spectroscopically similar fluorophores

The principle of time- and spectrally resolved confocal laser-scanning microscopy is described in **Figure 1**. For efficient excitation of a broad color palette of fluorophores, three alternatingly pulsed lasers emitting at 485 nm, 532 nm and 640 nm are used at a repetition rate of 13.3 MHz. The fluorescence signal is spectrally separated by a spectrograph and detected on a 32-channel array photomultiplier tube (PMT) using TCSPC.

In our first set of experiments, we selected fluorophores that could be efficiently excited at one of the three available laser wavelengths. For excitation at 485 nm, we selected a fluorescent protein (EGFP) and two organic fluorophores (ATTO 488 and Alexa Fluor 488) that share the same underlying rhodamine structure and consequently have almost identical spectroscopic characteristics (**Supplementary Table 1**). As free dyes in aqueous solution, ATTO 488 and Alexa Fluor 488 have absorption and emission maxima in the range of 490–500 nm and 515–521 nm, with mono-exponential fluorescence lifetimes of 4.07 ns and 4.16 ns, respectively. EGFP has very similar spectral characteristics but a shorter fluorescence lifetime of 2.71 ns (**Supplementary Table 1**). In addition, we used ATTO 490LS, an organic fluorophore with a Stokes shift of ~165 nm (**Supplementary Table 1**). ATTO 490LS can be easily identified by its red-shifted fluorescence emission and short fluorescence lifetime of 2.63 ns.

Discrimination of ATTO 488 and Alexa Fluor 488 is more challenging, especially because the spectroscopic characteristics of most organic dyes are sensitively influenced by their environment—specifically, the absorption and emission characteristics change slightly but unpredictably upon conjugation of the dye to antibodies or other biomolecules (**Supplementary Table 1**). Moreover, rhodamine and oxazine dyes in particular are prone to fluorescence quenching by electron donors such as the DNA nucleotide guanosine and the amino acid tryptophan via photoinduced electron transfer[33–36]. Therefore, conjugation of these dyes to antibodies or to the tryptophan-containing peptide phalloidin results in fluorescence quenching and complex multi-exponential fluorescence decays (**Supplementary Table 1**). Thus different biomolecules labeled with the same dye can exhibit different absorption and emission maxima as well as different fluorescence-decay patterns (**Supplementary Table 1**). We used ATTO 488 twice for specific labeling of two different target molecules to impede fluorophore identification and demonstrate the potential of the method. To generate fluorescence-emission and lifetime patterns, we labeled cells with each fluorescent probe separately.

In these experiments, we used EGFP fused to lamin C to label the nuclear envelope, ATTO 488–labeled phalloidin to label the actin skeleton, ATTO 488 azide to label nascent DNA by click chemistry, Alexa Fluor 488–labeled antibodies to label giantin in the Golgi, and ATTO 490LS–labeled antibodies to label fibrillarin in the nucleoli of U2OS cells (**Fig. 2**).

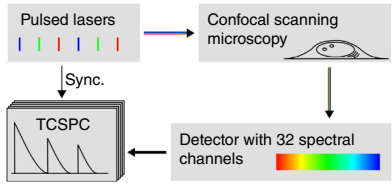

Figure 1 | Principle of sFLIM. The sample is excited by three pulsed lasers at 485 nm, 532 nm and 640 nm in an alternating scheme and scanned pixel by pixel. The fluorescent light is split into 32 spectral channels for recording of spectral information, and it is detected with TCSPC for extraction of lifetime information. The acquired multidimensional data (laser, spectral and lifetime) are then processed by the software. Sync., synchronization pulses for time measurements.

The slight differences in the absorption and emission spectra of the five fluorescent probes are reflected not only in the spectral information (**Fig. 2i**) but also in the different fluorescence intensities recorded after pulsed alternating excitation at 485 nm, 532 nm and 640 nm (**Fig. 2h**). Although the fluorescence lifetimes of ATTO 488–labeled phalloidin and nascent DNA differed only slightly (by ~100 ps) when the molecules were embedded in Mowiol (**Supplementary Table 1** and **Fig. 2h**), both targets could be readily identified (**Fig. 2b**). Even when all five fluorescent probes were used simultaneously, the pattern-matching algorithm unequivocally identified the contribution of each fluorophore per pixel. The resulting multicolor fluorescence images demonstrate specific labeling of five different cellular targets (**Fig. 2b**).

Next we performed multidimensional fluorescence imaging with fluorescent probes that could be efficiently excited at 532 nm (**Supplementary Table 1**). We used five probes: ATTO 520–labeled phalloidin for actin, mRFP-fibrillarin for nucleoli, Alexa Fluor 555–labeled antibodies for β-tubulin, Alexa Fluor 532–labeled antibodies for giantin, and MitoTracker Orange for mitochondria staining. Small differences in absorption and emission maxima (540–600 nm) and in fluorescence lifetime (1.7–3.1 ns) were sufficient for clear identification of the five different cellular targets (**Supplementary Fig. 1**). Finally, we used five fluorescent probes for simultaneous imaging with excitation at 640 nm: ATTO 655–labeled phalloidin for actin filaments, DRAQ5 for nuclear DNA, Alexa Fluor 633–labeled antibodies for fibrillarin, Alexa Fluor 647–labeled antibodies for tubulin, and Alexa Fluor 700–labeled antibodies for giantin (**Supplementary Table 1**). The lifetimes of these probes ranged from 0.5 ns to 2.0 ns (**Supplementary Fig. 2**). The results of these experiments demonstrate that our multidimensional sFLIM and pattern-matching approach is capable of simultaneous imaging of five different probes per excitation wavelength. We found that the identification precision decreased substantially when only spectral or lifetime information was used (**Supplementary Fig. 3**). Because the spectral assignment of patterns to the recorded signal is based mainly on the signal generated by the most efficient excitation laser (e.g., 640-nm excitation for the red dyes) (**Supplementary Fig. 3**), the technique enables parallel imaging of up to 15 cellular targets.

Visualization of nine different cellular structures

To demonstrate the potential of multi-target fluorescence imaging by sFLIM, we used the following fluorescent probes to label

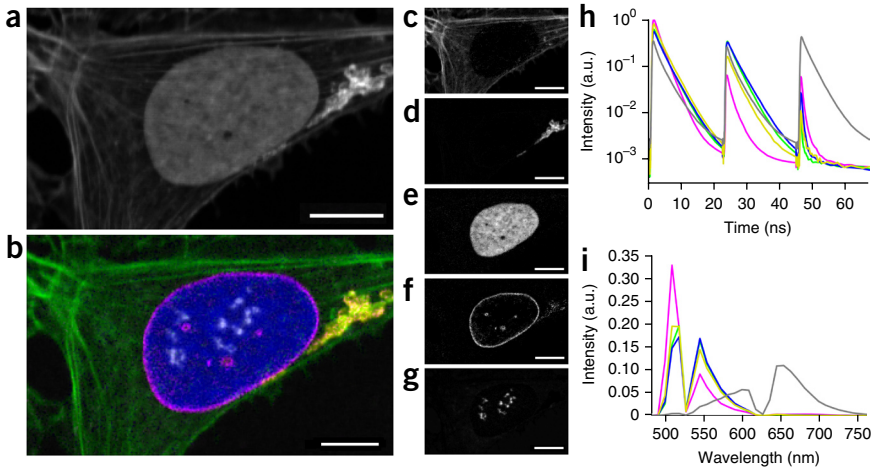

Figure 2 | Multi-target fluorescence imaging of five similar fluorescent probes. (**a**) Total fluorescence intensity image of an U2OS cell labeled with five fluorescent probes. (**b**–**g**) Resulting sFLIM composite image (**b**) showing F-actin stained with ATTO 488 phalloidin (green; **c**), Golgi stained with primary rabbit antibody to giantin and Alexa Fluor 488–labeled goat anti-rabbit secondary antibody (yellow; **d**), EdU (5-ethynyl-2'deoxyuridine; nascent DNA) inside the nucleus stained via click chemistry with ATTO 488 azide (blue; **e**), nuclear envelope stained via transfection of lamin C–EGFP (magenta; **f**), and nucleoli stained with primary mouse antibody to fibrillarin and ATTO 490LS–labeled goat anti-mouse secondary antibody (white; **g**). (**h**,**i**) The five corresponding reference patterns: (**h**) fluorescence decays corresponding to the three alternating laser pulses and (**i**) emission spectra with gaps determined by the filter system used to discriminate fluorescence from scattered light. The brightest pixels in **a**,**c**–**g** correspond to 5,488, 3,005, 4,573, 2,509, 483 and 293 photons. Color-coding in **h** and **i** corresponds to that in **b**. a.u., arbitrary units. Scale bars, 10 µm.

different cellular structures, with three probes used for each irradiation wavelength (**Fig. 3**): EGFP (lamin C), ATTO 488 azide (nascent DNA), ATTO 490LS (nucleoli), Alexa Fluor 532 (Golgi), Alexa Fluor 555 (microtubules), MitoTracker Orange (mitochondria), Alexa Fluor 647 (nuclear envelope), ATTO 655 phalloidin (F-actin) and DRAQ5 (DNA). The extracted single-target images (**Fig. 3c**–**k**) and the resulting composite image (**Fig. 3a**) clearly show that we were able to visualize nine different cellular structures simultaneously in a single experiment.

Multi-target fluorescence imaging with one fluorophore

To further increase the degree of difficulty, we labeled three different cellular structures—Golgi, nascent DNA and F-actin—with ATTO 488 (**Fig. 4**). As can be judged from the data in **Supplementary Table 1**, the spectral differences between the three fluorescent probes are negligible (**Fig. 4g**), and the fluorescence lifetimes show only small differences (**Fig. 4f**). Nevertheless, the pattern-matching technique enabled us to unequivocally identify the three slightly different fluorescence signals (**Fig. 4a**). In addition, we performed triple-labeling experiments using Alexa Fluor 647 and obtained similar results, which demonstrates the general applicability of the method (**Supplementary Fig. 4**).

In some triple-labeled cells (2× ATTO 488, 1× Alexa Fluor 488), we noticed vesicle-like spots outside of the nucleus that the pattern-matching algorithm assigned to DNA signals (**Supplementary Fig. 5**). We reasoned that the observed vesicles

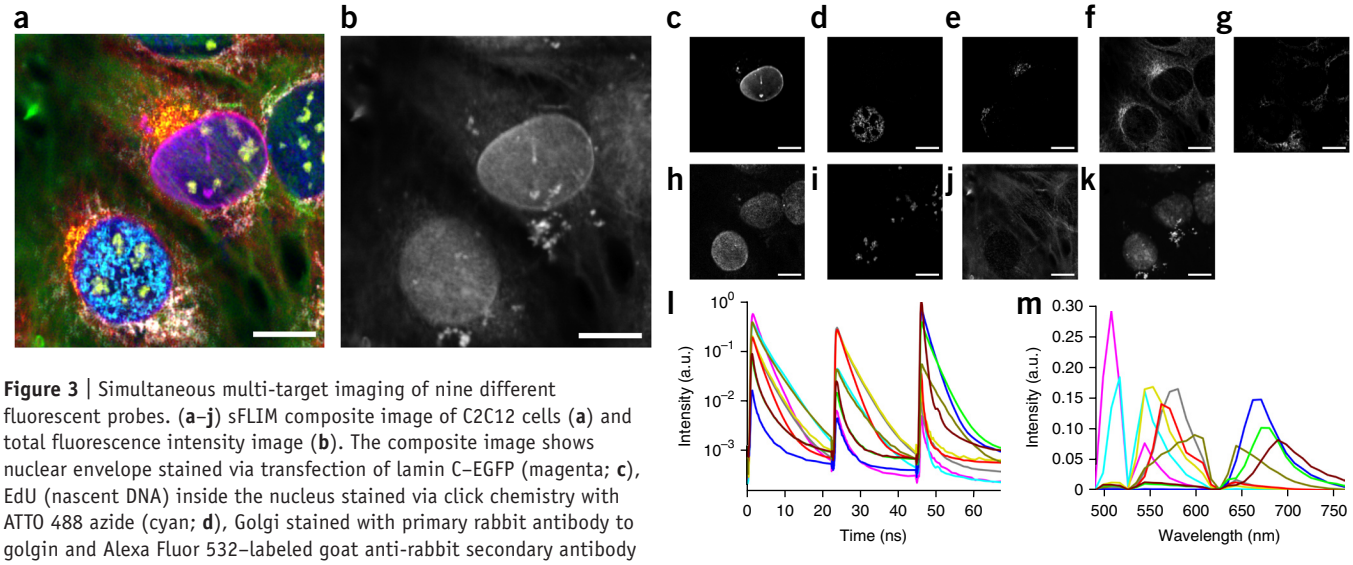

Figure 3 | Simultaneous multi-target imaging of nine different fluorescent probes. (**a**–**j**) sFLIM composite image of C2C12 cells (**a**) and total fluorescence intensity image (**b**). The composite image shows nuclear envelope stained via transfection of lamin C–EGFP (magenta; **c**), EdU (nascent DNA) inside the nucleus stained via click chemistry with ATTO 488 azide (cyan; **d**), Golgi stained with primary rabbit antibody to golgin and Alexa Fluor 532–labeled goat anti-rabbit secondary antibody (yellow; **e**), microtubules stained with Alexa Fluor 555–labeled rabbit anti–β-tubulin (red; **f**), mitochondria stained with MitoTracker Orange (white; **g**), nuclear envelope stained with primary guinea pig antibody to sun1 and Alexa Fluor 647–labeled goat anti–guinea pig secondary antibody (blue; **h**), nucleoli stained with primary mouse antibody to fibrillarin and ATTO 490LS–labeled goat anti-mouse secondary antibody (yellow-green; **i**), and F-actin stained with ATTO 655 phalloidin (green; **j**). (**k**) Nuclei were also stained with DNA-intercalating DRAQ5 (dark red in **l**,**m**; not shown in **a** for the sake of clarity). (**l**,**m**) The nine corresponding reference patterns: (**l**) fluorescence decays corresponding to the three alternating laser pulses and (**m**) emission spectra with gaps determined by the filter system used to discriminate fluorescence from scattered light. The brightest pixels in **b**–**k** correspond to 5,024, 2,090, 251, 157, 1,270, 828, 2,145, 458, 2,416 and 4,656 photons. Color-coding in **l** and **m** corresponds to that described for **a** and **k**. a.u., arbitrary units. Scale bars, 10 µm.

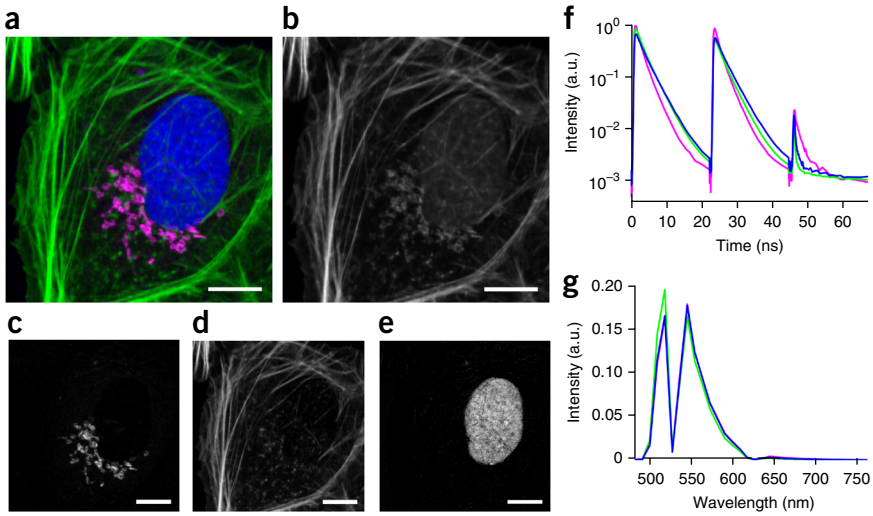

Figure 4 | Fluorescence imaging of three different cellular structures labeled with ATTO 488. (**a**–**e**) sFLIM composite image of a U2OS cell (**a**) and total fluorescence intensity image (**b**). Shown are Golgi stained with primary rabbit antibody to giantin and ATTO 488–labeled goat anti-rabbit secondary antibody (magenta; **c**), F-actin stained with ATTO 488 phalloidin (green; **d**), and EdU (nascent DNA) inside the nucleus stained via click chemistry with ATTO 488 azide (blue; **e**). (**f**,**g**) Fluorescence decays (**f**) and spectra (**g**) of the three ATTO 488–labeled probes. The brightest pixels in **b**–**e** correspond to 6,674, 2,663, 6,674 and 1,777 photons. Color-coding in **f** and **g** corresponds to that described for **a**. a.u., arbitrary units. Scale bars, 10 µm.

most likely represented free ATTO 488 azide molecules used for labeling of nascent DNA that accumulated nonspecifically in endosomes. Therefore, we introduced a new pattern generated only from the vesicle-like unspecific signals outside of the nucleus and repeated the pixel allocation. This allowed us to clearly distinguish the vesicle-like structures from the nascent DNA signals inside of the nucleus (**Supplementary Fig. 5**). These results show that the pattern-matching algorithm is capable of using even very small spectroscopic differences, such as the difference between free and clicked ATTO 488 azide, for signal identification. Thus the method could be used to discriminate the signals of fluorescent probes bound specifically to a target structure from the signals of nonspecific free fluorescent probes.

Taking advantage of the potential of the method to discriminate fluorescence signals on the basis of elemental differences in spectroscopic characteristics, we labeled cells with Mitotracker Orange and generated three different reference patterns from signals recorded from mitochondrial structures, vesicle-like spots (probably endosomes) in the cytoplasm, and nucleoli-like structures in the nucleus (**Supplementary Fig. 6**). The three patterns indeed showed slightly different fluorescence decay patterns and emission spectra that permitted the clear-cut identification of three different cellular structures: mitochondria, endosomes and nucleoli (**Supplementary Fig. 6**).

STED microscopy with spectrally similar dyes

Next we investigated whether sFLIM in combination with efficient pattern matching can be used for super-resolution imaging by STED microscopy, with which it is highly desirable to use only one depletion wavelength for imaging of different fluorophores. We selected the fluorophores Abberior STAR 635P and ATTO 647N, which are almost spectrally identical, for labeling of tubulin and Golgi structures in U2OS cells. The two fluorophores exhibit only small differences in fluorescence lifetime (in the range of a few hundred picoseconds in the cellular context) and minor differences in absorption and emission spectra (**Supplementary Table 1**). For efficient excitation of both fluorophores, we used pulsed lasers emitting at 640 nm and 660 nm. Stimulated depletion was achieved with a pulsed near-infrared STED laser emitting at 765 nm. The resulting STED microscopy images (**Fig. 5**) show well-separated Golgi and tubulin structures with improved resolution compared to diffraction-limited images, demonstrating that the two fluorophores could be unequivocally identified.

DISCUSSION

Our data clearly demonstrate the potential of multi-target fluorescence imaging by sFLIM. The possibility of using spectrally similar fluorophores to image different cellular structures opens up useful new applications of sFLIM, such as its combination with STED microscopy to obtain super-resolution images of multiple species using a single depletion laser[37,38]. The method might also

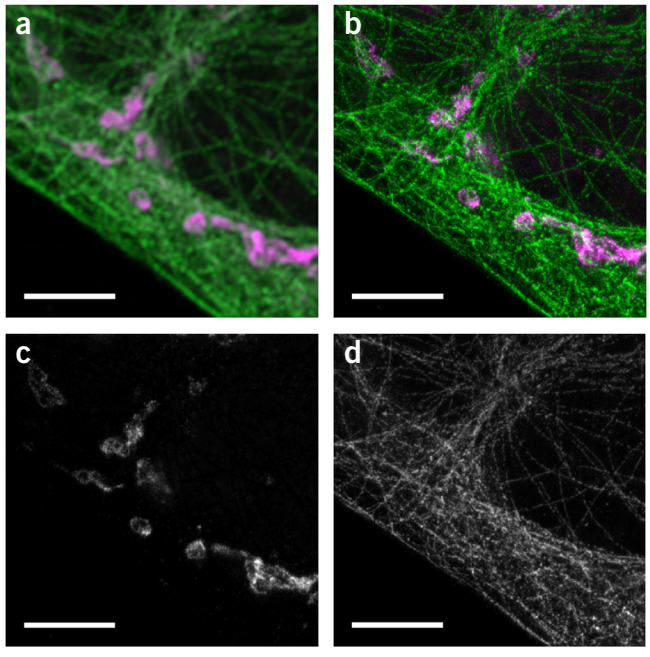

Figure 5 | Two-color super-resolution STED imaging. (**a**–**d**) Classical confocal fluorescence image (**a**) and STED image (**b**) of U2OS cells stained with two similar fluorophores. Structures are clearly separated even in the super-resolved images. Shown are Golgi stained with primary rabbit antibody to giantin and ATTO 647N–labeled goat anti-rabbit secondary antibody (magenta; **c**) and microtubules stained with primary mouse antibody to β-tubulin and Abberior STAR 635P–labeled goat anti-mouse secondary antibody (green; **d**). Photon counts in the brightest pixels were around 5,000 (**c**) and 10,000 (**d**). Scale bars, 5 µm.

be useful for investigating aspects of the local nano-environment in living cells—for example, intracellular pH differences could be studied using pH-sensitive GFP derivatives[39]. The quality of multi-target fluorescence imaging strongly depends on the labeling specificity and efficiency; this creates a challenge, as each target usually requires a special staining protocol for optimal labeling efficiency and structure preservation. Therefore, aspects of the labeling protocol such as labeling order and concentration have to be carefully optimized in all multi-target experiments.

Because the reliability of the described algorithm depends on many parameters in a highly nonlinear way, it is not possible to give an analytical expression for the error of the method. The main parameters that can be influenced by the experimentalist are the number of photons collected (integration time) and the shape of the patterns to be separated (choice of fluorophores). With this in mind, we carried out a simulation study in which we added varying amounts of three experimentally determined patterns (**Supplementary Note 1**). The results show that unmixing of three components can be achieved for very moderate photon numbers even in the absence of spectral information. The accuracy achieved was very close to a brute-force minimum search of the maximum likelihood value, which resembles the absolute optimum achievable outcome[28] (**Supplementary Note 1** and **Supplementary Figs. 7–9**). Extending the previously described pattern-matching algorithm[20] to include spectral information allows unmixing of more components with higher accuracy.

To estimate how much the retrieved amplitudes for each pattern depend on variations of the shape (i.e., the quality of the pattern), we used different sets of pixels from different regions of labeled cells (Golgi, nascent DNA and F-actin labeled with ATTO 488; **Fig. 4**) to generate a set of slightly different reference patterns for each fluorescent component and calculated the mean and s.d. of the patterns from each set. The results show that the s.d. was on the order of 1% of the maximum amplitude of the mean pattern (**Supplementary Fig. 10**). To find out how much the amplitudes retrieved by the algorithm depended on the shape of the pattern, we analyzed the amplitude of the respective component in each pixel of the image. As a reference, we used the amplitudes that were obtained using the mean patterns for each component. When we used the mean pattern plus or minus the s.d. instead of the reference pattern, maximum average deviations on the order of 5% resulted; this demonstrates that our method is nonproblematic and behaved linearly within the scope of our analysis (**Supplementary Fig. 11**).

We also analyzed an additional set of independently acquired patterns for Golgi, nascent DNA and F-actin labeled with ATTO 488 and compared the resulting changes in signal assignment with the data in **Figure 4**. Here the mean deviation per pixel was only up to 0.8% of the brightest pixel of the corresponding structure (**Supplementary Fig. 12**). The results were of similar quality for patterns generated from very bright and dim regions (**Supplementary Fig. 13**), indicating that autofluorescence and TCSPC pileup do not deteriorate data analysis. However, if inappropriate patterns are used (e.g., from older samples; Online Methods), signal assignment will be defective (**Supplementary Fig. 14**).

Comparison with other algorithms demonstrated the superior performance of our pattern-matching approach (**Supplementary Note 2**). In addition, for measurements with readily distinguishable fluorescent probes, such as the STED measurement with two fluorophores (**Fig. 5**), a simpler algorithm can compute comparable results in a much shorter time (**Supplementary Note 3**).

METHODS

Methods and any associated references are available in the online version of the paper.

Note: Any Supplementary Information and Source Data files are available in the online version of the paper.

ACKNOWLEDGMENTS

We thank T. Krüger and M. Alsheimer (Department of Cell and Developmental Biology, Biozentrum Universität Würzburg, Würzburg, Germany) for providing plasmids and antibodies. This work was supported by the Biophotonics Initiative of the German Bundesministerium für Bildung und Forschung (BMBF grants 13N10432 and 13N12781 to T.N., A.L. and M.S.).

AUTHOR CONTRIBUTIONS

T.N., A.L., I.G., M.S. and B.K. designed experiments. T.N., A.L., I.G., B.K., H.-J.R., M.P. and F.K. generated and processed data. T.N., A.L., J.E., I.G., B.K. and M.S. wrote, edited and approved the final draft of manuscript.

COMPETING FINANCIAL INTERESTS

The authors declare no competing financial interests.

1. Lichtman, J.W. & Conchello, J.A. Fluorescence microscopy. *Nat. Methods* **2**, 910–919 (2005).
2. Minsky, M. Microscopy apparatus. US patent 3,013,467 (1961).
3. Pawley, J.B. (ed.) *Handbook of Biological Confocal Microscopy* 3rd edn. (Springer, 2006).
4. Denk, W., Strickler, J.H. & Webb, W.W. Two-photon laser scanning microscopy. *Science* **248**, 73–76 (1990).
5. Tsien, R.Y. The green fluorescent protein. *Annu. Rev. Biochem.* **67**, 509–544 (1998).
6. Shaner, N.C., Steinbach, P.A. & Tsien, R.Y. A guide to choosing fluorescent proteins. *Nat. Methods* **2**, 905–909 (2005).
7. Keppler, A. *et al.* A general method for the covalent labeling of fusion proteins with small molecules *in vivo*. *Nat. Biotechnol.* **21**, 86–89 (2003).
8. Miller, L.W. & Cornish, V.W. Selective chemical labeling of proteins in living cells. *Curr. Opin. Chem. Biol.* **9**, 56–61 (2005).
9. Johnson, I. & Spence, M.T.Z. (eds.) *The Molecular Probes Handbook: A Guide to Fluorescent Probes and Labeling Technologies* 11th edn., (2010).
10. Moerner, W.E. & Orrit, M. Illuminating single molecules in condensed matter. *Science* **283**, 1670–1676 (1999).
11. Weiss, S. Fluorescence spectroscopy of single biomolecules. *Science* **283**, 1676–1683 (1999).
12. Jameson, D.M. & Ross, J.A. Fluorescence polarization/anisotropy in diagnostics and imaging. *Chem. Rev.* **110**, 2685–2708 (2010).
13. Liyanage, M. *et al.* Multicolour spectral karyotyping of mouse chromosomes. *Nat. Genet.* **14**, 312–315 (1996).
14. Garini, Y., Gil, A., Bar-Am, I., Cabib, D. & Katzir, N. Signal to noise analysis of multiple color fluorescence imaging microscopy. *Cytometry* **35**, 214–226 (1999).
15. Tsurui, H. *et al.* Seven-color fluorescence imaging of tissue samples based on Fourier spectroscopy and singular value decomposition. *J. Histochem. Cytochem.* **48**, 653–662 (2000).
16. Bastiaens, P.I. & Squire, A. Fluorescence lifetime imaging microscopy: spatial resolution of biochemical processes in the cell. *Trends Cell Biol.* **9**, 48–52 (1999).
17. Chang, C.W., Sud, D. & Mycek, M.A. Fluorescence lifetime imaging microscopy. *Methods Cell Biol.* **81**, 495–524 (2007).
18. Elangovan, M., Day, R.N. & Periasami, A. Nanosecond fluorescence resonance energy transfer—fluorescence lifetime imaging microscopy to localize the protein interactions in a single living cell. *J. Microsc.* **205**, 3–14 (2002).
19. Wahl, M., Koberling, F., Patting, M., Rahn, H. & Erdmann, R. Time-resolved confocal fluorescence imaging and spectroscopy system with single molecule sensitivity and sub-micrometer resolution. *Curr. Pharm. Biotechnol.* **5**, 299–308 (2004).

20. Gregor, I. & Patting, M. Pattern-based linear unmixing for efficient and reliable analysis of multicomponent TCSPC data. In *Advanced Photon Counting: Applications, Methods, Instrumentation* (eds. Kapusta, P., Wahl, M. & Erdmann, R.) 241–263 (Springer, 2015).
21. Tinnefeld, P., Herten, D.P. & Sauer, M. Photophysical dynamics of single dye molecules studied by spectrally-resolved fluorescence lifetime imaging microscopy (SFLIM). *J. Phys. Chem. A* **105**, 7989–8003 (2001).
22. Knemeyer, J.P., Herten, D.P. & Sauer, M. Detection and identification of single molecules in living cells using spectrally-resolved fluorescence lifetime imaging microscopy (SFLIM). *Anal. Chem.* **75**, 2147–2153 (2003).
23. Heilemann, M. *et al.* Multistep energy transfer in single molecular photonic wires. *J. Am. Chem. Soc.* **126**, 6514–6515 (2004).
24. Becker, W. *et al.* Fluorescence lifetime images and correlation spectra obtained by multidimensional time-correlated single photon counting. *Microsc. Res. Tech.* **69**, 186–195 (2006).
25. Fereidouni, F., Reitsma, K. & Gerritsen, H.C. High speed multispectral fluorescence lifetime imaging. *Opt. Express* **21**, 11769–11782 (2013).
26. Enderlein, J. *et al.* A maximum likelihood estimator to distinguish single molecules by their fluorescence decays. *Chem. Phys. Lett.* **270**, 464–470 (1997).
27. Lieberwirth, U. *et al.* Multiplex dye DNA sequencing in capillary gel electrophoresis by diode laser-based time-resolved fluorescence detection. *Anal. Chem.* **70**, 4771–4779 (1998).
28. Enderlein, J. & Sauer, M. Optimal algorithm for single-molecule identification with time-correlated single-photon counting. *J. Phys. Chem. A* **105**, 48–53 (2001).
29. Hanley, Q.S. Spectrally-resolved fluorescent lifetime imaging. *J. R. Soc. Interface* **6** (suppl. 1), S83–S92 (2009).
30. Zhou, Y., Dickenson, J.M. & Hanley, Q.S. Imaging lifetime and anisotropy spectra in the frequency domain. *J. Microsc.* **234**, 80–88 (2009).
31. Fereidouni, F., Bader, A.N. & Gerritsen, H.C. Spectral phasor analysis allows rapid and reliable unmixing of fluorescence microscopy spectral images. *Opt. Express* **20**, 12729 (2012).
32. Klar, T.A., Jakobs, S., Dyba, M., Egner, A. & Hell, S.W. Fluorescence microscopy with diffraction resolution barrier broken by stimulated emission. *Proc. Natl. Acad. Sci. USA* **97**, 8206–8210 (2000).
33. Knemeyer, J.P., Marmé, N. & Sauer, M. Probes for detection of specific DNA sequences at the single molecule level. *Anal. Chem.* **72**, 3717–3724 (2000).
34. Heinlein, T., Knemeyer, J.P., Piestert, O. & Sauer, M. Nucleobase-specific quenching of fluorescent dyes in DNA-hairpins. *J. Phys. Chem. B* **107**, 7957–7964 (2003).
35. Marmé, N., Knemeyer, J.P., Wolfrum, J. & Sauer, M. Inter- and intramolecular fluorescence quenching of organic dyes by tryptophan. *Bioconjug. Chem.* **14**, 1133–1139 (2003).
36. Doose, S., Neuweiler, H. & Sauer, M. A close look at fluorescence quenching of organic dyes by tryptophan. *ChemPhysChem* **6**, 2277–2285 (2005).
37. Donnert, G. *et al.* Two-color far-field fluorescence nanoscopy. *Biophys. J.* **92**, L67–L69 (2007).
38. Meyer, L. *et al.* Dual-color STED microscopy at 30-nm focal-plane resolution. *Small* **4**, 1095–1100 (2008).
39. Schmitt, F.-J. *et al.* eGFP-pHsens as a highly sensitive fluorophore for cellular pH determination by fluorescence lifetime imaging microscopy (FLIM). *Biochim. Biophys. Acta* **1837**, 1581–1593 (2014).

ONLINE METHODS

Sample preparation. *Cell culture.* Mouse C2C12 cells and human U2OS cells (CLS Cell Lines Service; 400476 and 300364, respectively) were authenticated by the supplier. We tested the cells for mycoplasma contamination by PCR and immunofluorescence. We cultured the cells in DMEM (PAA; D6546) with 10% fetal calf serum, 100 U/ml penicillin, 100 µg/ml streptomycin, and 1 mM L-glutamine (PAA). The cells were allowed to grow on coverslips at 37 °C and 5% CO_2 for at least 2 d.

Transfection. For transfection of lamin C–GNAEGR–EGFP[40] (M. Alsheimer, Biozentrum Universität Würzburg) and fibrillarin-mRFP (T. Krüger, Biozentrum Universität Würzburg), after 24 h of cell growth on coverslips, we transfected the cells with FuGene HD (Promega), following the instructions of the supplier. We dissolved the transfection mix in DMEM (without fetal calf serum, penicillin or streptomycin) and incubated the cells for another 24 h at 37 °C and 5% CO_2 before further fixation or labeling procedures.

EdU treatment. For integration of EdU (5-ethynyl-2′deoxyuridine; Life Technologies) into nascent DNA, after 24 h of cell growth on coverslips, we treated the cells with EdU (1:1,000) for 24 h. In cases of transfection, we added EdU immediately after transfection. Alternatively, to stain only very newly synthesized DNA, we added EdU only for the 2 h immediately before fixation (**Fig. 3d**).

Labeling of mitochondria. We used MitoTracker Orange (Life Technologies; M7511) to label mitochondria. We incubated the cells for 40 min at 37 °C and 5% CO_2 with 500 nM MitoTracker Orange before fixation.

Fixation and permeabilization. We rinsed the cells in PBS (37 °C), fixed them for 15 min at 37 °C with 4% (wt/vol) formaldehyde in PBS, rinsed them in PBS again, permeabilized them for 8 min in 0.1% (wt/vol) Triton X-100 in PBS at room temperature, washed them for 5 min in PBS, saturated them with 5% (wt/vol) BSA in PBS for at least 20 min, and rinsed them briefly in PBS before subsequent incubations.

Immunofluorescence and F-actin labeling with phalloidin. We incubated the cells in PBS with primary antibodies for 45 min, washed them in PBS for at least 5 min, incubated them in PBS with dye-coupled secondary antibodies for 30 min, and washed them in PBS for at least 10 min. To avoid cross-reactions, we performed the direct immunofluorescence with antibodies to α- or β-tubulin for 45 min after the indirect immunofluorescence was completed. We either added dye-coupled phalloidin to the secondary antibody mix for simultaneous incubation or incubated the cells with dye-coupled phalloidin for at least 30 min in single stains. Antibody concentrations, suppliers and catalog numbers are listed in **Supplementary Table 2**.

Labeling of DNA by click chemistry (EdU). We used the ClickOx protocol[41] for EdU-treated cells after all other labeling procedures were complete. The reaction mix contained 100 mM Tris with HCl (pH 8.5), 100 mM ascorbic acid (from sodium ascorbate), 1–2 mM $CuSO_4$, 1% (wt/vol) glucose, 1% (wt/vol) glycerol, 2 U glucose oxidase, 40 U catalase, and about 8 µM dye-coupled azide (ATTO 488 azide, ATTO-TEC, AD 488-101; Alexa Fluor 647 azide, Life Technologies, C10340), and the reaction was carried out for 10 min in the dark. We added ascorbic acid as the last reagent, because it starts the reaction. After rinsing the samples in PBS, we incubated them in 10 mM EDTA in PBS for 5 min.

DRAQ5. After all other stainings were complete, we incubated the cells with 1 µM DRAQ5 in PBS (Cell Signaling Technology; 4084S) for 5 min and then washed them for at least 10 min in PBS.

Post-fixation and embedding of cells. After all labeling steps were completed, we post-fixed the cells for 5 min with 4% (wt/vol) formaldehyde in PBS, washed them in PBS for at least 5 min, and embedded them in Mowiol (Carl Roth; 0713).

Antibody labeling. We labeled goat anti-mouse $F(ab')_2$ fragments (Life Technologies, A10534) with ATTO 490LS NHS (ATTO-TEC, AD 490LS-31) in the presence of 50 mM $NaHCO_3$ at pH 8.3 with an incubation time of 1 h. We purified the product with NAP-5 columns (Sephadex G-25, GE Healthcare) and determined the degree of labeling to 2.6 and the concentration to 2.45 µM using standard absorbance spectroscopy.

Measurement of spectroscopic characteristics. We measured spectroscopic characteristics of free fluorophores and fluorescent probes (**Supplementary Table 1**) in cuvettes at a concentration of ~1 µM in PBS (pH 7.4). We used a V-650 spectrophotometer (Jasco) to determine absorption maxima and an FP-6500 spectrofluorometer (Jasco) for emission and excitation maxima. We measured fluorescence lifetimes with a FluoTime 200 time-resolved spectrometer (PicoQuant) and analyzed the results with FluoFit 4.4.0.1 software (PicoQuant). We fitted lifetimes from sFLIM measurements with Gnuplot.

Fibrillarin-mRFP. We detached about 1×10^6 U2OS cells transfected with fibrillarin-mRFP (described above) from their substrate, concentrated them with a centrifuge (200*g*) and lysed them with 0.5% (wt/vol) Triton X-100 in PBS for 20–25 min on ice. We mixed the product with about an equal amount of PBS, incubated it with 50 U DNase I (Roche) and 5 mM $CaCl_2$ for 40 min at room temperature, and then centrifuged it again (200*g*). We used the supernatant for measurements.

Isolation of DNA. We treated about 1×10^6 U2OS cells with EdU and clicked them with ATTO 488 azide or Alexa Fluor 647 azide (described above). We purified the DNA with a kit (nexttec 1-Step DNA Isolation Kit, Tissue & Cells, Biozym, 391010N) and then used it for measurements. A control with U2OS cells treated in the same way but without EdU showed no significant fluorescence. We also used the DNA isolation kit to obtain untreated DNA. For DRAQ5 measurements, we added 4.5 nmol of DRAQ5 to the DNA of about 4×10^5 cells.

Experimental setup. *Confocal measurements.* We carried out sFLIM measurements on a confocal time-resolved microscope (MicroTime 200, PicoQuant) equipped with a piezo-driven scanning stage for objective scanning (Physik Instrumente). For excitation we used three pulsed lasers with wavelengths of 485 nm, 532 nm and 640 nm (LDH-D-C-485, LDH-P-FA-530B and LDH-D-C-640, respectively; PicoQuant). We operated the lasers in a pulsed interleaved excitation (PIE) mode with a repetitive three-color pulse train. The 485-nm laser pulse was followed by pulses at 532 nm and finally 640 nm. We set the time between two subsequent pulses to 25 ns. The irradiation power of the different lasers was determined by the different labeling efficiencies but was always on the same order of magnitude. For the separation of excitation and fluorescence, we applied a wavelength-independent beam splitter (20% reflection and 80% transmission; AHF Analysentechnik AG). We investigated the specimen with a

60× oil-immersion objective (PLAPON 60XOTIRFM, Olympus Europe). We focused the fluorescence light emitted by the sample onto a 50-µm-diameter pinhole and guided it with a 50-µm–core diameter multimode optical fiber (AMS AG) to the external sFLIM detection system. For quick preselection of suitable cells in the sample, we used epifluorescence illumination with an EMCCD (electron-multiplying charge-coupled device) camera (Andor Ltd.).

The sFLIM detection system comprised a spectrograph equipped with a custom fiber port and multichannel array PMT detection as well as a specially modified TCSPC unit. We collimated the fluorescence light emitted from the fiber. The light then passed three notch filters designed to suppress specifically the three excitation wavelengths used (AHF Analysentechnik AG). We used a grating spectrograph (Shamrock SR-163, Andor Ltd.) to disperse the light spectrally and image it onto a 32-channel array PMT equipped with cylindrical microlenses (Hamamatsu Photonics Deutschland; H7260-20MOD). We used a grating with 600 l/mm and 500-nm blaze (Andor Ltd.; SR1-GRT-0600-0500). In this way the array PMT covered a spectral region from 482 nm to 773 nm with wavelength steps of 9.4 nm between successive channels. We cooled the array PMT to a temperature of 15 °C to reduce background noise to around 500 counts per second per channel. A custom-designed single photon–detection module registered the spectral channel for each detected photon. In addition, we amplified a summed signal from the last PMT dynode to deliver information about photon-arrival timing. We fed both signals into a modified HydraHarp 400 TCSPC system (PicoQuant) equipped with one TCSPC channel. Because of the modification of the HydraHarp 400 module, the channel routing information was included in the TTTR (time-tagged, time-resolved) data format to record the timing and channel information for the detected photons. In addition, we recorded marker signals from the piezo controller to generate spatial information. The sFLIM detection system including fiber delivery, spectrograph and array PMT achieved a measured detection efficiency of 4% (red) to 10% (green detection wavelength region) and a timing resolution of 270 ps full-width at half-maximum (instrument response function (IRF)), including the laser pulse width. We used the software SymPhoTime (PicoQuant) for data acquisition, online FLIM visualization and simple fluorescence decay analysis. To reduce the number of modifications to the recorded TCSPC histograms due to pileup, we limited the total maximum count rate of all channels to 4 MHz. The pileup constraint is one factor that limits the speed of acquisition. However, compared with classical TCSPC hardware, which is subject to the 0.1% pileup rule, the new PicoQuant TCSPC card HydraHarp 400 is less susceptible to pileup effects, because the signal pulse (fluorescence photons) and synchronization pulse are detected asynchronously in independent channels. We took images 50 µm × 50 µm (300 × 300 pixels) in size with a pixel dwell time of 1.2 ms, resulting in a total image-acquisition time of 340 s and typically up to 5,000 photons in the brightest image pixels. After briefly evaluating the multichannel FLIM images with the SymPhoTime software, we analyzed the recorded TTTR raw image files using a specially developed pattern-matching software written with Matlab (MathWorks).

The main drawbacks of this setup are the relatively low detection efficiency and the limited speed of acquisition. Possible ways to overcome these limits in the future include the application of detection arrays with higher sensitivity (e.g., multi-array PMTs with GaAsP cathodes). The acquisition speed could be further enhanced by the use of TCSPC devices equipped with parallel and independent time-to-digital converter modules for each channel. In such a case each channel could record the maximum count rate given by the pileup limit, allowing much higher overall count rates.

STED measurements. We carried out STED measurements with the MicroTime 200 STED system (PicoQuant). We used a piezo-driven scanning stage for objective scanning (Physik Instrumente). For excitation we applied two pulsed lasers emitting at wavelengths of 640 nm and 660 nm, respectively (LDH-D-C-640 and LDH-D-C-660, respectively; PicoQuant). We achieved stimulated depletion with a pulsed near-infrared STED laser emitting at 765 nm (VisIR-765 STED, PicoQuant). We operated the laser at a repetition rate of 10 MHz and with an average power of 40 mW measured before the light entered the objective. We operated the lasers in PIE mode with a repetitive two-color pulse train. We optimized the timing of the excitation pulses with respect to the STED laser for optimal depletion results. We set the time between two subsequent laser pulses to 100 ns. We guided the STED and excitation lasers in the same single-mode fiber to the main optical unit. For separation of excitation and fluorescence, we used a customized major dichroic (zt640/752rpc, AHF Analysentechnik AG). Between the major dichroic and the objective, we applied a segmented phase plate to achieve a donut-shaped intensity profile for 765 nm; the 640-nm and 660-nm excitation beams were left unaffected (EASYDOnut phase plate, 640/765 nm, Abberior). We investigated the specimen with a 100× oil-immersion objective (UPlanSAPO 100X, Olympus Europe). The fluorescence light emitted by the sample passed two detection filters (RazorEdge LP-664-RU and 697/58-BrightLine-HC, AHF Analysentechnik AG) and was focused onto a 50-µm-diameter pinhole to enable confocal detection. The light was then split onto two single-photon avalanche diode (SPAD) detectors (τ-SPAD, PicoQuant) using a dichroic beam splitter (T-685-LPXR, AHF Analysentechnik AG). For quick preselection of suitable cells in the sample, we used epifluorescence illumination with a CMOS (complementary metal-oxide semiconductor) CCD camera (UI-3370CP-NIR-GL, IDS Imaging Development Systems). We fed the signals of both SPAD detectors into a HydraHarp 400 TCSPC system (PicoQuant). We used the SymPhoTime 64 software (PicoQuant) for data acquisition, online STED image visualization and pattern-matching analysis. We acquired images 17.3 µm × 17.3 µm (500 × 500 pixels) in size with a pixel dwell time of 1.0 ms, resulting in a total image-acquisition time of 5 min.

Creation of reference patterns. To generate reference patterns, we imaged singly stained cells with the described setup. For the best results, we selected only regions with adequate fluorescence originating from the stained structure. We merged the information of all photons in these pixels into one multidimensional reference pattern, including excitation laser, spectral detection channel, and the shape of the time-dependent fluorescence decay. With this approach it is important that all conditions (i.e., cell type, staining procedure (including click chemistry treatment), laser power, temperature and optical adjustment) be the same as for the multistained samples. Samples should be as fresh as

doi:10.1038/nmeth.3740

possible or at least of the same age, as sometimes we observed that patterns changed in aging samples, most probably because of dehydration and decomposition of the cellular samples, and that these changes were accompanied by increased autofluorescence. All these requirements are automatically fulfilled if patterns are selected from unequivocally identified singly stained parts of multistained images.

Pattern-matching data-analysis algorithm. We basically follow the previously described procedure to analyze multicomponent TCSPC data[20]. However, instead of using only the temporal signal, here we also have to consider the spectral dependency. We presume that the detection probability of a given fluorophore is given as the normalized probability density function $p(t,\lambda)\ dtd\lambda$, which describes how many photons per time interval dt and spectral window $d\lambda$ are expected from the fluorophore. We refer to this function as the pattern of the fluorophore.

When a sample containing multiple fluorophores is measured, the temporally and spectrally resolved measurement will provide a superposition $I(t,\lambda)\ dtd\lambda$ of individual patterns:

$$I(t,\lambda)dtd\lambda = \sum_i n_i p_i(t,\lambda)dtd\lambda \qquad (1)$$

where n_i denotes the amount of fluorophore i. In pixel-wise sampled measurement of an inhomogeneous specimen, a typical task is finding the respective n_i in each pixel.

All meaningful values of the variables in equation (1) are positively constricted. The exponential temporal decay characteristics of the patterns and the Poisson statistics of the signal noise prevent a straightforward solution of equation (1).

Description of the algorithm. *Preparation of the raw data.* Following ref. 20, we first bin the temporal data into bins 32 ps wide and align the time axis of the data such that the IRF has its center of gravity at 1 ns for all detection channels. Second, the data are rebinned to a multiple-tau scale,

$$\tau_j = \delta \begin{cases} 1 & j < 33 \\ 2^{\lfloor (j-33)/8 \rfloor} & \text{Else} \end{cases} \qquad (2)$$

using a base resolution of $\delta = 32$ ps. This binning substantially reduces the photon noise in the time bins distant from the excitation pulse. This processing of the data has to be done only once after the recording of the data.

Optimization and data preparation for pattern analysis. Depending on the set of patterns P_i, we now process the preconditioned data. We aim to reduce the number of data bins in order to reduce the noise, as the noise is dependent on the signal itself rather than on the sampling bandwidth. Therefore, we compress the data in both the spectral and the temporal dimension. We first compute the spectra $s_i(\lambda)\ d\lambda$ of the patterns $P_i\ (t,\lambda)\ dtd\lambda$ by summing over the temporal coordinate.

For binning we add up all spectral channels, where the order of the three biggest amplitudes of the spectra is the same. This gives us a spectrally compact representation $T_i(t,l)\ dtd\lambda_l$ of the patterns $P_i(t,\lambda)\ dtd\lambda$. Finally, we transform the data in the temporal dimension using a similar approach.

Here we start by adding all temporal bins up to 1 ns (center of the IRF). For all later bins, we also look for the order of the three biggest amplitudes and sum up all bins that show the same order. This kind of binning is done for all spectral channels, individually. This gives the final representation $R_i(k,l)\ dt_k d\lambda_l$ of the patterns.

Data recorded after different excitation pulses (PIE experiments) are processed in the same way. The data in the individual pixels are binned identically to the pattern data.

Having found the transformed representation of the pixel data, we now search for a solution of equation (1) for any pixel by minimizing the Kullback-Leibler discrepancy Δ_{KL} (ref. 42).

$$\Delta_{KL} = \sum_b \tilde{I} - \hat{I} + \hat{I}(\ln \hat{I} - \ln \tilde{I}), \text{ with } \hat{I} = \mathbf{R}\hat{\mathbf{n}} \qquad (3)$$

The minimum of equation (3) is equivalent to the maximum likelihood for data showing a Poissonian noise figure. A positively defined solution can be found via an algorithm described by Lee and Seung[43] that has been applied to similar problems[44]. Starting from a suitably chosen (positively confined) starting vector $\hat{\mathbf{n}}$, we determine the local gradient. The increment of the coordinate vector is chosen such that it can be expressed as a multiplication with a positively constrained scaling vector γ: $\hat{\mathbf{n}}_{i+1} = \gamma \hat{\mathbf{n}}_i$. The presented algorithm looks for the best linear combination of the selected patterns to resemble the pixel data. If the patterns do not entirely match the recorded data, the found solution will naturally be biased. The crucial task of finding and selecting the set of patterns falls to the user.

Code availability. The source code for the software used to analyze the data is provided with the **Supplementary Software**. Updated software, source code and sample data for three different cellular structures labeled with ATTO 488 are available at https://idefix.biozentrum.uni-wuerzburg.de/~thonie/sFLIM_software_sampledata/.

40. Alsheimer, M., von Glasenapp, E., Schnölzer, M., Heid, H. & Benavente, R. Meiotic lamin C2: the unique amino-terminal hexapeptide GNAEGR is essential for nuclear envelope association. *Proc. Natl. Acad. Sci. USA* **97**, 13120–13125 (2000).
41. Löschberger, A., Niehörster, T. & Sauer, M. Click chemistry for the conservation of cellular structures and fluorescent proteins: ClickOx. *Biotechnol. J.* **9**, 693–697 (2014).
42. Kullback, S. & Leibler, R.A. On information and sufficiency. *Ann. Stat.* **22**, 79–86 (1951).
43. Lee, D.D. & Seung, H.S. Algorithms for non-negative matrix factorization. In *Advances in Neural Information Processing Systems* 13 (eds. Leen, T.K., Dietterich, T.G. & Tresp, V.) 556–562 (MIT Press, 2000).
44. Neher, R.A. *et al.* Blind source separation techniques for the decomposition of multiply labeled fluorescence images. *Biophys. J.* **96**, 3791–3800 (2009).